Two-Dimensional Fluid Model Simulation of Bell Jar Top Inductively Coupled Plasma

Han-Ming Wu, Ben W. Yu, Ming Li, and Yun Yang

Abstract—**In the present paper, argon (Ar) plasmas in a bell jar inductively coupled plasma (ICP) source are systematically studied over pressures from 5 to 20 mtorr and power inputs from 0.2 to 0.5 kW. In this study, both a two-dimensional (2-D) fluid model simulation and global model calculation are compared. The 2-D fluid model simulation with a self-consistent power deposition is developed to describe the Ar plasma behavior as well as predict the plasma parameter distributions. Finally, a quantitative comparison between the global model and the fluid model is made to test their validity.**

Index Terms—**Inductively coupled plasma, simulation**

I. INTRODUCTION

THE limitations of radio frequency (RF) diodes have led to the development of new plasma sources, such as electron cyclotron resonance (ECR) plasma source and inductively coupled plasma (ICP) sources that operate at low pressure and high plasma density. Plasma densities in these enhanced plasma sources can reach to $10^{11}\sim10^{12}$ cm^3 with neutral pressures in the range of $1\sim20$ mtorr [1], [2]. As a new kind of plasma source, ICP is appealing due to its structural simplicity [3]. Accompanying the development of this new generation of plasma sources has been an effort to understand plasma parameters in ICP [4]–[8].

Low-pressure ICP has been employed for etching processing for the last few years. This has prompted research on these sources by many groups [9]–[16]. In order to further develop this etching tool and provide predictions for design, we have been carrying out several studies of ICP [3]–[8]. Our latest ICP source design employs bell jar quartz top sources to reduce the thickness of dielectric quartz. Meanwhile, the bell jar cover can sustain much higher pressure with less thickness.

II. THEORETICAL MODELING

A. Reactor Configuration

The geometry of the bell jar top ICP chamber is shown in Fig. 1. The bottom chamber is made of stainless steel with radius $r = 12$ cm and height $L = 8$ cm, respectively. The top bell jar cover, with curvature radius 13 cm, is isolated, whereas the bottom chamber is grounded. The dome cover is made of quartz with 0.5-cm thickness [8].

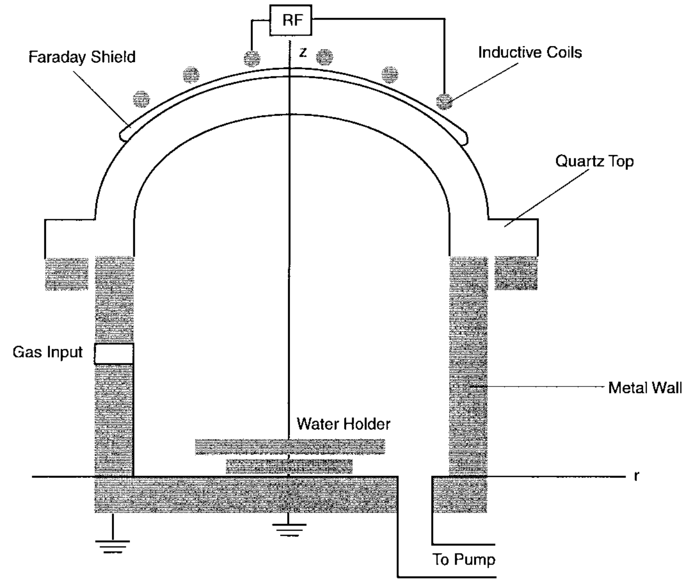

Fig. 1. The geometry of the ICP chamber.

B. Global Model

A global model developed by Lieberman and Gottscho has proved to be a reliable and simple method to estimate plasma parameters in an enhanced plasma source [1], [4]. The global model calculation for the dome top ICP was previously done. For clarity, a brief introduction to the global model follows.

Rate coefficients for inelastic process are assumed to have the same form

$$K_i(T_e) = \sigma_i v_e \exp\left(\frac{-E_i}{kT_e}\right) \quad (1)$$

where σ_i and $v_i = (\frac{8kT_e}{\pi m_e})^{\frac{1}{2}}$ are the cross section for inelastic process i and mean electron thermal speed, respectively. The subscript i denotes the ith inelastic process

$$K_{iZ}NnV = \Gamma \equiv \Gamma_b + \Gamma_s + \Gamma_t. \quad (2)$$

The global particle balance requires K_{iZ}, N, n, V, Γ_b, Γ_s, and Γ_t are the ionization rate, the neutral gas density, the plasma density, the chamber volume, the ion fluxes at the

Manuscript received May 11, 1995; revised October 7, 1996. This work was supported by the Chinese Academy of Sciences under the Presidential Foundation.

H.-M. Wu and B. W. Yu are with CFD Research Corporation, Huntsville, AL 35805 USA (e-mail: hmw@cfdrc.com).

M. Li is with the Department of Chemical Engineering, University of California, Berkeley, CA 94720 USA.

Y. Yang is with the Institute of Mechanics, Chinese Academy of Sciences, Beijing 100080, China.

Publisher Item Identifier S 0093-3813(97)00683-8.

0093–3813/97$10.00 © 1997 IEEE

Authorized licensed use limited to: THE LIBRARY OF CHINESE ACADEMY OF SCIENCES. Downloaded on November 5, 2009 at 03:27 from IEEE Xplore. Restrictions apply.

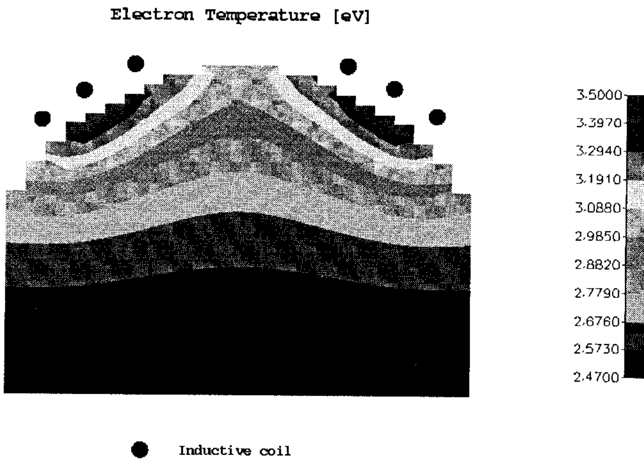

Fig. 2. Spatial profile of electron temperature with respect to the 10-mtorr and 200-W input.

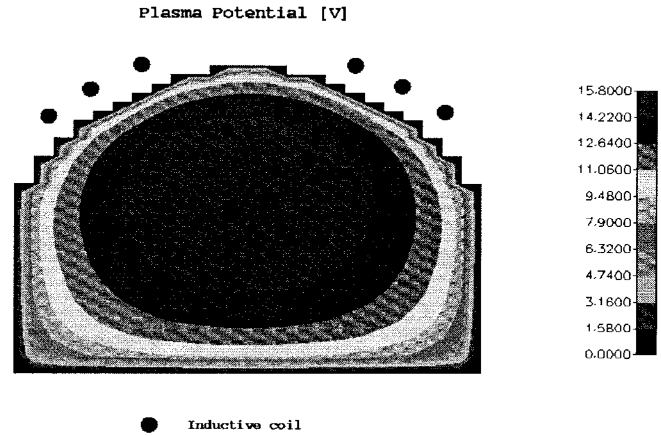

Fig. 3. Spatial profile of plasma potential with respect to the 10-mtorr and 200-W input.

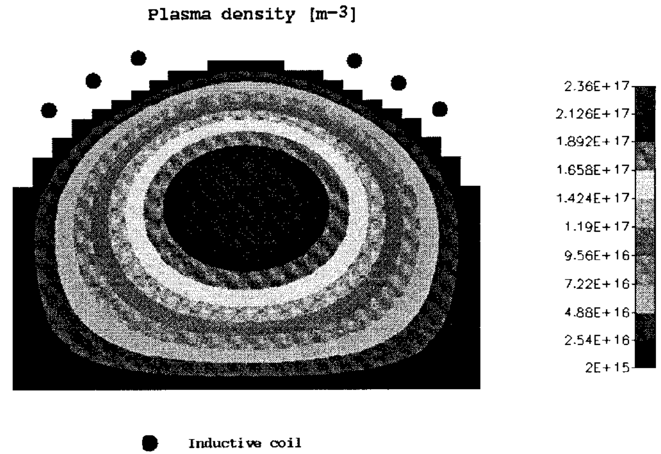

Fig. 4. Plasma density contours with respect to the 10-mtorr and 200-W input.

bottom of the wall, side wall, and top dome wall, respectively. These fluxes can be expressed as

$$\begin{aligned}\Gamma_b &= \pi r^2 h_L n u_b, \quad \Gamma_s = 2\pi r L h_R n u_b \\ \Gamma_t &= \int_s n u_B (h_L \cos\theta + h_R \sin\theta) ds \\ &= 2\pi R^2 n u_B \int_s (0.5 h_L \sin 2\theta + h_R \sin^2\theta) d\theta \\ &= \pi R^2 n u_B (\alpha h_L + 2 b h_R)\end{aligned} \tag{3}$$

where $a = \int_s \sin 2\theta d\theta = 0.85$, $b = \int_s \sin\ ^2\theta d\theta = 0.41$, and the integral domain, s is the top sperical surface, respectively; $u_B = \sqrt{\frac{k\Gamma_e}{\pi m_e}}$ is the Bohm velocity and

$$h_L = 0.86\left(3 + \frac{0.5L}{\lambda_i}\right)^{-\frac{1}{2}}, \quad h_R = 0.8\left(4 + \frac{r}{\lambda_i}\right)^{-\frac{1}{2}} \tag{4}$$

where $\lambda_i = \frac{1}{\sigma_i n}$ is the ion-neutral mean free path.

Electron temperature T_e can be obtained by means of solving the following equation:

$$\frac{K_{iZ}(T_e)}{u_B} = \frac{\Gamma}{u_B N n V} \equiv N d_{\text{eff}} \tag{5}$$

where

$$d_{\text{eff}} = \frac{V}{\pi[h_L(r^2 + R^2 a) + 2h_R(rL + R^2 b)]}.$$

Plasma density n and ion current density on wafer J_b can be derived in the following procedure: Define the collisional energy lost per electron-ion pair created

$$\varepsilon_c = \varepsilon_{\text{ion}} + \frac{[K_{\text{ex}}\varepsilon_{\text{ex}} + K_{me}\varepsilon_{me} + K_{el}\varepsilon_{el}]}{K_{\text{ion}}} \tag{6}$$

where $\varepsilon_{\text{ion}} = 15.75$ eV, $\varepsilon_{\text{ex}} = 14.1$ eV, $\varepsilon_{me} = 12$ eV, and $\varepsilon_{el} = 3mkT_e/M$ are the energies lost per electron, for argon (Ar), as a result of ionization, electronic excitation, metastable creation, and elastic collisions, respectively. The total energy lost per electron-ion pair in the system can be expressed as follows:

$$\varepsilon_L = \varepsilon_c + 5.2kT_e + 2kT_e = \varepsilon_c + 7.2kT_e. \tag{7}$$

The overall global energy balance for the ICP can be written in terms of ε_L

$$P_{\text{abs}} = u_B n_s A_{\text{eff}} \varepsilon_L \tag{8}$$

where

$$n_s A_{\text{eff}} = \pi n r^2 h_L + 2r\pi n L h_R + \int_s n(h_L \cos\theta + h_R \sin\theta)\, d\theta$$

P_{abs} is power absorbed in the plasma and n_s the plasma density at the presheath, respectively. Then

$$n = \frac{P_{\text{abs}}}{\left\{e u_\beta \varepsilon_L \left[\pi r^2 h_L + 2r^2 L h_R + \int_s (h_L \cos\theta + h_R \sin\theta)\, d\theta\right]\right\}} \tag{9}$$

can directly be solved for plasma density.

C. 2-D Fluid Model

1) Fluid Equations: The basic assumptions of the model are: 1) the neutral gas flow is omitted; 2) the ion temperature is the same as neutral gas; 3) the inductive coils are simplified as three coaxial circular coils; 4) the electron distribution

Authorized licensed use limited to: THE LIBRARY OF CHINESE ACADEMY OF SCIENCES. Downloaded on November 5, 2009 at 03:27 from IEEE Xplore. Restrictions apply.

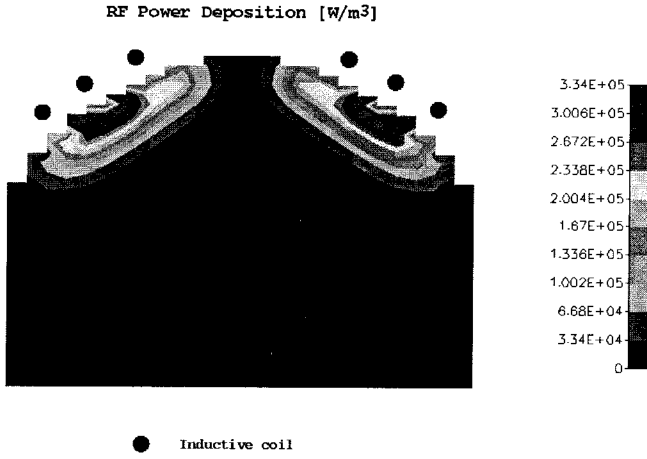

Fig. 5. Inductive RF power deposition profile with respect to the 10-mtorr and 200-W input.

is assumed to be Maxwellian; and 5) neutral density and temperature are assumed to be uniform in the chamber.

Three neutral argon gas pressures, 5, 10, and 20 mtorr, are considered separately in the simulation. The total power inputs are 200 W and 500 W, respectively.

The time average equations for electrons and ions are

$$\nabla \cdot \boldsymbol{J}_e = R_i \tag{10}$$

$$\nabla \cdot \boldsymbol{J}_i = R_i \tag{11}$$

$$\nabla \cdot \boldsymbol{Q}_e = q_j - \Sigma R_k \varepsilon_k e \tag{12}$$

where

$$\boldsymbol{J}_e = -\mu_e n_e \boldsymbol{E}_s - \left(\frac{k}{m_e \nu_{eN}}\right) \nabla (n_e T_e)$$

$$\boldsymbol{J}_i = -\mu_i n_i \boldsymbol{E}_s - \left(\frac{2k}{m_i \nu_{iN}}\right) \nabla (n_i T_i)$$

$$\boldsymbol{Q}_e = 2.5(kT_e \boldsymbol{J}_e) - 2.5\left(\frac{k^2}{m_e \nu_{eN}}\right) n_e T_e \nabla T_e$$

$$\mu_e = \frac{e}{m_e \nu_{eN}}, \quad \mu_i = \frac{2e}{m_i \nu_{iN}}$$

$$q_j = \frac{1}{T \int_T \sigma E^2 dt}.$$

The total input power can be written as

$$P_t = 2\pi \int\int q_j r dr dz. \tag{13}$$

The collision rate R_k can be expressed as $R_k = K_k n_e N$, where the subscript $k = iz$, ex, me, and el have the same definitions as (4). The above set of fluid equations is closed with Poisson's equation with regard to the space charge to the electrostatic potential

$$\varepsilon_0 \nabla^2 \phi = e(n_e - n_i) \tag{14}$$

where ε_0 is the permittivity of free space.

The boundary conditions are the same as our previous work, i.e., $n_e = \phi = n \cdot \nabla n_i = n \cdot \nabla T_e = 0$ on the metallic wall; on the axis there are $\partial n_e / \partial_r = \partial n_i / \partial r = \partial \phi / \partial r = \partial T_e / \partial r = 0$. Based on the thin plasma sheath model, we have the analytical results to obtain the boundary conditions on the quartz wall as following:

$$\begin{aligned} J_{ew} &= \frac{1}{4} n_{es} v_{es} \exp\left(\frac{-e\Delta\phi}{kT_e}\right) \\ J_{iw} &= n_{is} u_B \\ \phi_w &= \phi_s + \left(\frac{kT_{es}}{e}\right) \ln\left(\frac{4J_{iw}}{n_{es} v_{es}}\right) \end{aligned} \tag{15}$$

where J_{ew} and J_{iw} are their normal components to the wall, the subscript s represents the plasma-sheath boundary position, boundary plasma potential $\Delta\phi = \phi_w - \phi_s$ and the electron energy flux on the top $Q_{ew} = J_{ew}(2kT_{es} + e\Delta\phi)$, respectively.

2) Electromagnetic Equations: The electric field consists of inductively coupled field and plasma static field. The net field is $\boldsymbol{E} = \boldsymbol{E_I} + \boldsymbol{Ep}$. The plasma static field is determined by Poisson is equation

$$\nabla^2 \phi = -\nabla \cdot E = \frac{-e}{\varepsilon_0}(n_i - n_e). \tag{16}$$

Because of the axial symmetry assumption, the inductive electric field, which has only an azimuthal component, is written as

$$E = E_1 \cos \omega t + E_2 \sin \omega t. \tag{17}$$

The equations for E are

$$\nabla^2 E_1 - \frac{E_1}{r^2} + \left(\frac{\omega^2}{c^2} - \frac{\xi \sigma \omega^2}{\nu_{eN}}\right) E_1 - \xi \sigma \omega E_2 = 0 \tag{18}$$

$$\nabla^2 E_2 - \frac{E_2}{r_2} + \left(\frac{\omega^2}{c^2} - \frac{\xi \sigma \omega^2}{\nu_{eN}}\right) E_2 + \xi \sigma \omega E_1 = 0 \tag{19}$$

where $\xi = 4\pi + 10^{-7} H/m$

$$\sigma = \left(\frac{n_e e^2}{m_e \nu_{eN}}\right) \left[1 + \left(\frac{\omega}{\nu_{eN}}\right)^2\right]$$

is plasma electric conductivity, ν_{eN} is the electron-neutral collision frequency. The boundary condition for (12) and (13) are $E = 0$ on the metallic wall and the axis. The boundary condition on the quartz bell jar is determined by the coil current $I = I_0 \cos \omega t$ and the inductive plasma current $\sigma_{ij}, E_{1,2} \Delta z_i \Delta r_j$ at the nearest cell to wall. The detail deductive expression and computational method can be found from [7].

D. Results and Discussion

Fig. 2 is the electron temperature distribution with 10-mtorr neutral pressure and 200-W power input. As our prevous results show, T_e is quite uniform in the bulk plasma.

The difference between maximum on the upper centerline and minimum at the bottom is less than 1.0 eV. With this relatively flat temperature profile, we can expect the spatial profiles for ionization rate and plasma density be quite similar. The plasma potential is shown in Fig. 3. It can be seen that the

Authorized licensed use limited to: THE LIBRARY OF CHINESE ACADEMY OF SCIENCES. Downloaded on November 5, 2009 at 03:27 from IEEE Xplore. Restrictions apply.

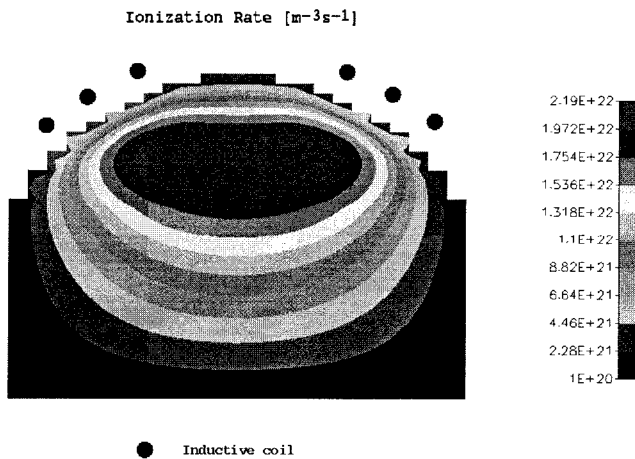

Fig. 6. Ionization rate distribution with respect to the 10-mtorr and 200-W input.

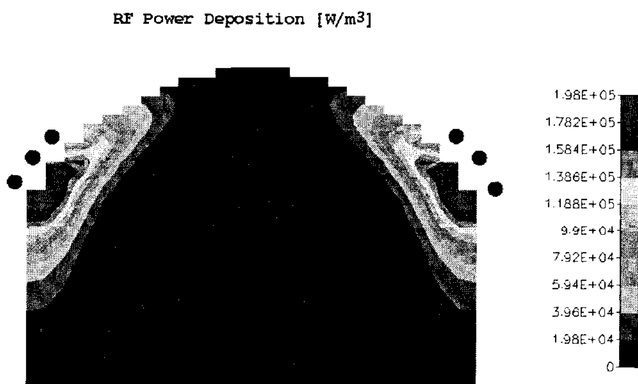

Fig. 7. Inductive RF power deposition profile with wide coils, where $p = 10$ mtorr and $P_{abs} = 200$ W.

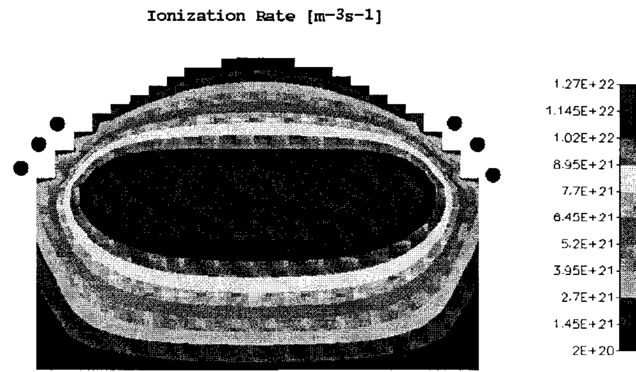

Fig. 8. Ionization rate distribution with wide coils, where $p = 10$ mtorr and $P_{abs} = 200$ W.

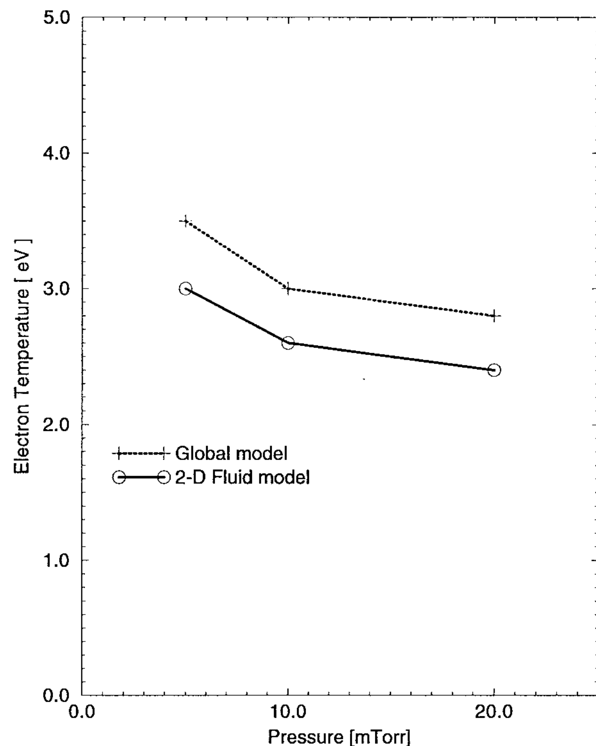

Fig. 9. T_e comparison of global model and simulation $P_{abs} = 200$ W.

maximum at the center is about 15.8 V and the minimum is at the corner. It implies that the plasma static electric field E_p is small. Fig. 4 is the plasma density contours with the same operation condition. The plasma density near the bottom is quite uniform. This is one of the characteristics for the bell jar top ICP. It is found that the maximum exceeds 2×10^{17} m^3. Fig. 5 shows contours of RF power deposition. It is obvious that most power is concentrated near the coils on the top. In Fig. 6, there is an ionization rate distribution. Since ionization is a function of power deposition, electron temperature, and electron density, the contours seem to be a compromise of these parameters.

To see the coil geometry effects, Figs. 7 and 8 are of power deposition, ionization rate, and plasma density with respect to wider inductive coils case. It seems that the wider coil can result in the more uniform parameter distribution. It is well known that the higher the neutral pressure, the more localized parameter distribution. Therefore, as the neutral pressure is increased the parameters, such as n_e and R_{iZ}, would have two off-axis-peak values [17]. These coil geometry effects depend on the chamber shape, discharged gas species, total power input, as well as neutral pressure. There is no simple way to predict the plasma uniformity for common plasma tools. Therefore, to carry on some numerical simulations for special plasma tools are inevitable to most design of plasma sources.

Fig. 9 is the comparison for electron temperatures between the global model and the simulation. The plasma densities comparison between global model and simulation is shown in Fig. 10. It seems that the simulation agrees reasonably well with the global model. The difference might come from the neutral gas uniformity assumption. The global model can give a quick estimation whereas the fluid can provide a spatial profile for parameters.

It is well known that the uniformity in a flat ICP is primarily determined by the inductive coil geometry. However, in the bell jar top ICP, there are two ways to improve the

Authorized licensed use limited to: THE LIBRARY OF CHINESE ACADEMY OF SCIENCES. Downloaded on November 5, 2009 at 03:27 from IEEE Xplore. Restrictions apply.

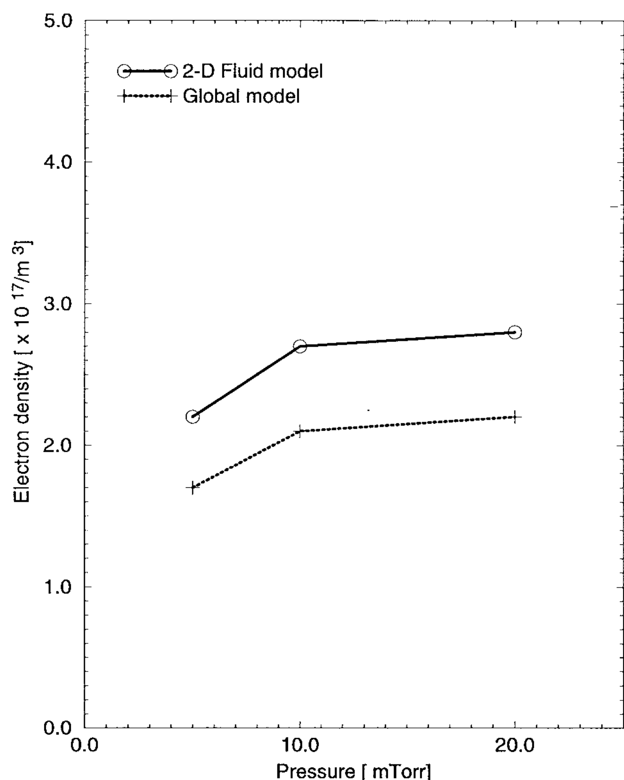

Fig. 10. n_e comparison of global model and simulation $P_{abs} = 200$ W.

plasma parameters. The one is to adjust the inductive coil configuration and the other is to change the stage position. Therefore, the uniformity in the bell jar top ICP can be improved. In addition to the uniformity, it is obvious that the bell jar top quart can be easy made due to the thinner thickness. Experimental measurement for plasma parameters, by means of a tuned Langmuir probe, is in progress and will be published soon.

III. CONCLUSION

The modeling seems quite reliable after the comparison to the global model results. It paves a way to optimize the plasma parameter distribution for design work. The bell jar top ICP has the advantage of reducing the thickness of quartz to sustain relative high pressure. For large area ICP sources, the quartz thickness becomes larger and it would result in long-time heating to reach a steady state temperature in the quartz roof. It seems one of the advantages of a bell jar top ICP. This advantage can be generalized to some other plasma sources, such as ECR and helions. It is likely that a uniform plasma can be generated by means of adjusting both wafer stage position and inductive coil geometry. The detail work on the chamber geometry effect and coil geometry effects is still to be investigated. The comparison with the experimental data is going to be submitted for publication.

REFERENCES

[1] M. A. Lieberman and R. A. Gottscho, "Design of high density plasma sources for material processing," in *Physics of Thin Films*, M. Francombe and J. Vossen, Eds. New York: Academic, 1994.

[2] D. B. Graves, "Plasma processing," *IEEE Trans Plasma Sci.*, vol. 22, p. 31, Feb. 1994.

[3] H.-M. Wu, D. W. Dong, and J. Y. Xu, "Comparison between ICP and ECR," *Material of Electr.,* vol. 12, no. 7, 1994.

[4] R. Stewart, P. Vitello, and D. B. Graves, "2-D fluid simulation of high-density inductively coupled plasma sources," *J. Vac. Sci. Technol.,* vol. B12, p. 478, 1994.

[5] J. H. Keller, J. C. Forster, and M. S. Barnes, "Novel rf induction plasma processing techniques," *J. Vac. Sci. Technol.*, vol. A11, p. 2487, 1993.

[6] J. Hopwood, "Ion bombardment energy distribution in rf induction plasma," *Appl. Phys. Lett.*, vol. 62, p. 640, 1993.

[7] M. Li, H.-M. Wu, and Y.-M. Chen, "2-D simulation of inductive plasma sources with self-consistent power deposition," *IEEE Trans. Plasma Sci.,* vol. 23, no. 4, p. 558, 1995.

[8] H.-M. Wu, M. Li, and Y.-M. Chen, "Parameter estimation of bell jar ICP," *Chinese Phys. Lett.*, vol. 12, no. 5, p. 281, 1995.

[9] "Transformer couple plasma reactor," U.S. patent no. 4 948 458, Aug. 1990.

[10] R. Piejak, V. Godyak, and B. Alexandrovich, "Magnetic field distribution measurement in low-pressure inductive discharge," *J. Appl. Phys.*, vol. 78, no. 9, p. 5296, 1995.

[11] P. L. G. Ventzek, M. Grappenhaus, and M. J. Kushner, "2-D modeling of high plasma density inductive sources for material processing," *J. Vac. Sci. Technol*., vol. B12, no. 6, p. 3118, Nov./Dec. 1994.

[12] T. Hori, M. D. Bowden, K. Uchino, K. Muraoka, and M. Maeda, "Measurement of electron temperature, electron density, and neutral density in ICP," to be published in *J. Vac. Sci. Technol.*

[13] D. P. Lymberopoulos and D. J. Economou, "2-D simulation of polysilicon etching with chlorine in high density plasma reactor," *IEEE Trans. Plasma Sci.*, vol. 12, no. 4, p. 537, Aug. 1995.

[14] K. Greenberg, Sandia Natl. Lab., private communication.

[15] V. I. Kolobov and V. A. Godyak, "Nonlocal electron kinetics in collisional gas discharge plasma," *IEEE Trans. Plasma Sci.*, vol. 23, no. 4, p. 503, Aug. 1995.

[16] L. J. Mahoney, A. E. Wendt, E. Barriros, C. J. Rechards, and J. L. Shohet, "Magnetic field distribution measurement in low-pressure inductive discharge," *J. Appl. Phys.* vol. 76, p. 2041, 1994.

[17] P. Vitello, Lawrence Livermore Natl. Lab., private communication.

Han-Ming Wu received the Ph.D. degree in 1987 from the Institute of Mechanics, Chinese Academy of Sciences, Beijing, China.

He joined CFD Research Corporation, Huntsville, AL, in 1995 and now is carrying on the project of ICP modeling. He has been interested in plasma assisted material processing research work, such as ECR and ICP research both in theoretical and experimental areas.

Ben W. Yu received the B.S. degree from Huazhong University of Science and Technology, Wuhan, China, in 1982. He received the M.S. and Ph.D. degrees in mechanical engineering from the University of Minnesota, Minneapolis–St. Paul, in 1989 and 1994, respectively.

In 1994 he joined CFD Research Corporation, Huntsville, AL, where he has been the Principal Investigator on DARPA-funded research projects such as materials processing plasmas, plasma equipment modeling, and particle contaminants in plasmas. His research work has included chemical vapor deposition of diamond thin films and thermal plasmas.

Authorized licensed use limited to: THE LIBRARY OF CHINESE ACADEMY OF SCIENCES. Downloaded on November 5, 2009 at 03:27 from IEEE Xplore. Restrictions apply.

Ming Li received the B.S. degree from Beijing University of Aeronautics and Astronautics and the M.S. degree in fluid dynamics from the Institute of Mechanics, Chinese Academy of Sciences, Beijing, China, in 1988 and 1991, respectively.

Since he joined the plasma division of the Institute of Mechanics in 1991, he has engaged in the numerical simulations of plasma and the study on particle-plasma interaction. In February 1995, he joined the Department of Chemical Engineering, University of California at Berkeley as a Visiting Researcher, and now he is carrying on the research of high-density plasma models and simulations.

Yun Yang received the B.S. degree in physics from Yunnan University, Kunming, China, in 1986 and the M.S. and Ph.D. degrees in material physics from Beijing Science and Technology University, Beijing, China, in 1989 and 1994, respectively.

In 1994, he joined the Plasma Division of the Institute of Mechanics, Chinese Academy of Sciences, China. His research interests include the plasma assisted materials processing, modeling plasma processing equipment, and other related topics in semiconductor etching.

Authorized licensed use limited to: THE LIBRARY OF CHINESE ACADEMY OF SCIENCES. Downloaded on November 5, 2009 at 03:27 from IEEE Xplore. Restrictions apply.